Invited Paper

Soft matter design principles for inorganic photonic nanoarchitectures in photovoltaics, colorimetric sensing and self-cleaning antireflective coatings

S. Guldin[a] and U. Steiner[b]

[a]Institute of Materials, École Polytechnique Fédérale de Lausanne, Lausanne, 1015, CH
[b]Department of Physics, University of Cambridge, JJ Thomson Ave, Cambridge CB30HE, UK

ABSTRACT

The self-assembly of soft matter, such as block copolymers or colloids, allows fine tuning of structure formation on the 10 - 500 nm length scale and therefore enables the design of materials with tunable optical response. We present strategies on how to exploit these formation principles to assemble inorganic nanoarchitectures with distinct optical properties and point out promising applications in photovoltaics, colorimetric sensing and self-cleaning antireflective coatings.

Keywords: antireflective coating, block copolymer, Bragg reflector, photonic architectures, photonic crystal, photovoltaics, porosity, self-assembly

1. INTRODUCTION

Soft nanotechnology relies on the self-assembling nature of synthetically designed building blocks to enable bottom-up morphology control on the nanometre scale.[1] The macromolecular tool box is rich in variety and relies on weak, non-covalent, intermolecular forces for the cooperative assembly of molecular building blocks into ordered superstructures. With adequate compatibilization, organic self-organization can also be used to structure-direct inorganic materials by co-assembly in a host-guest approach.[2,3] In this perspective, we want to outline how soft matter design principles can be employed for the fabrication of porous thin film architectures with a tunable photonic response.

An overview of key requirements are shown in Figure 1a. Simultaneous control over these will be crucial for applications discussed in the following. A central role in our soft matter-based design route plays the block copolymer (BCP) poly(isoprene-*block*-ethylene oxide) (PI-*b*-PEO). In the herein presented co-assembly approach (Figure 1a), the polymer acts as a host for the inorganic guest material. Upon adequate compatibilization, the inorganic guest preferentially interacts and coordinates with the PEO block, and therefore takes part in the self-organization process. In the right solvent, PI-*b*-PEO forms micelles with PI-cores in solution. Film processing, solvent evaporation, annealing of the inorganic material and subsequent removal of the organic host then gives rise to a nanoscopic inverse opal-type structure of densely packed pores in an inorganic matrix. As shown in Figure 1c, the resulting porous architectures are highly ordered and well interconnected. The average pore size is a direct consequence of the molecular weight of the PI block in the organic host and thus can be finely controlled. In the example shown here a molecular weight M_n of $8.2\,\mathrm{kg\,mol^{-1}}$ led to a mean pore size of 33 ± 6 nm, while M_n $28.6\,\mathrm{kg\,mol^{-1}}$ resulted in a pore size distribution of 52 ± 6 nm. This is in good agreement with scaling laws for the radius of gyration in a polymer melt. One core challenge in a co-assembly route to porous thin films is the material shrinkage that occurs during the processing, mostly due to the evaporation of residual solvents and condensation of the inorganic network (Figure 1d). We have recently developed a temperature annealing protocol that allows to accommodate material shrinkage, enables for multilayer processing and prevents the formation of cracks even in μm thick films.[4] Besides the ability to precisely tune the pore size in a well accessible and highly ordered network architecture, the co-assembly route also allows to manipulate the refractive index of the

Further author information:
S.G.: E-mail: Stefan.Guldin@epfl.ch, Telephone: +41 21 6937877
U.S.: E-mail: u.steiner@phy.cam.ac.uk , Telephone: +44 1223 337390

Micro- and Nanotechnology Sensors, Systems, and Applications VI, edited by Thomas George, M. Saif Islam, Achyut K. Dutta, Proc. of SPIE Vol. 9083, 908320 · © 2014 SPIE
CCC code: 0277-786X/14/$18 · doi: 10.1117/12.2050011

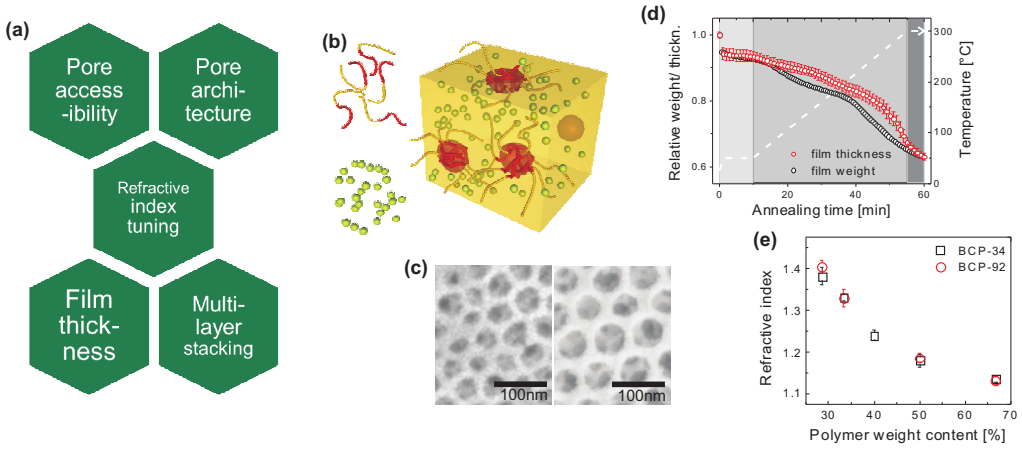

Figure 1. **Inorganic photonic nanoarchitectures by BCP co-assembly.** **(a)** Overview of key requirements for porous thin film architectures with tunable photonic responsive. **(b)** Schematic of BCP co-assembly. The polymer acts as a host for the inorganic material in the material self-organization, which is here a micellization process. Film processing, solvent evaporation, annealing of the inorganic material and subsequent removal of the organic host then gives rise to a nanoscopic inverse opal-type structure of densely packed pores in an inorganic matrix. **(c)** Resulting pore size in silica-type films in dependence of the molecular weight of the organic host PI-*b*-PEO. A molecular weight M_n of 8.2 kg mol^{-1} leads to a pore size distribution of 33 ± 6 nm, while M_n 28.6 kg mol^{-1} results in 52 ± 6 nm. **(d)** Material shrinkage due to evaporation of residual solvents and condensation of the inorganic network requires thin film annealing to prevent cracks. Here, the relative weight and thickness is shown during a typical annealing protocol. **(e)** Dependence of the refractive index ($\lambda = 632$ nm) of the resulting porous film as a function of polymer weight content in the initial mixture for two different BCPs. *b) Reproduced with permission from reference.*[7] *Copyright 2010 American Chemical Society. c), e) Adapted with permission from reference.*[8] *Copyright 2013 American Chemical Society. d) Adapted with permission from reference.*[4] *Copyright 2012 Wiley.*

porous film over a wide range. Shown in Figure 1e, this is a direct consequence of the mixing ratio of organic and inorganic components in the initial solution. A refractive index window of $1.4 < n < 1.13$ here corresponds to a porosity value ranging from 20 % to 73 %. It is important to note that the use of PI-*b*-PEO largely differs from widely established structure-directing agents such as PEO-*b*-PPO-*b*-PEO (pluronic). Previous BCP-based approaches were limited by extremely long fabrication times and limitations in porosity variation.[5,6] The present route is fundamentally different due the high Flory-Huggins interaction parameter of the isoprene and ethylene oxide blocks, their low glass-transition temperatures, and the high molecular weight, enabling greatly improved processing and structural control.

2. SOFT MATTER DESIGN PRINCIPLES FOR COLORIMETRIC SENSING

We have elucidated in the previous section how BCP co-assembly allows fine control over pore size, porosity and pore accessibility in thin films and enables multilayer stacking. With this tool box, we were able to introduce a novel materials route to mesoporous distributed Bragg reflectors (MDBRs).

MDBRs are defined as porous multilayer stacks of alternating high and low refractive index. Multiple interference of light reflected at each of the layer interfaces results in a characteristic reflection and transmission behavior that can be finely tuned by varying the refractive index, the thickness and the number of the alternating layers.[9,10] The combination of a DBR with accessible pores on the 10 nm length scale opens up a number of new and unique applications in biological and chemical sensing. Adsorption and desorption of gas phase molecules in the pores results in reversible changes of the refractive index of the building blocks, and thus, a modification of the characteristic optical properties.[5,11] When functionalized to bind specific molecules, MDBRs have been successfully used as biosensors at pico- to femtomolar concentrations to detect small organic molecules such as biotin and digoxigenin, DNA oligomers as well as proteins, including streptavidin and antibodies.[12] An array of

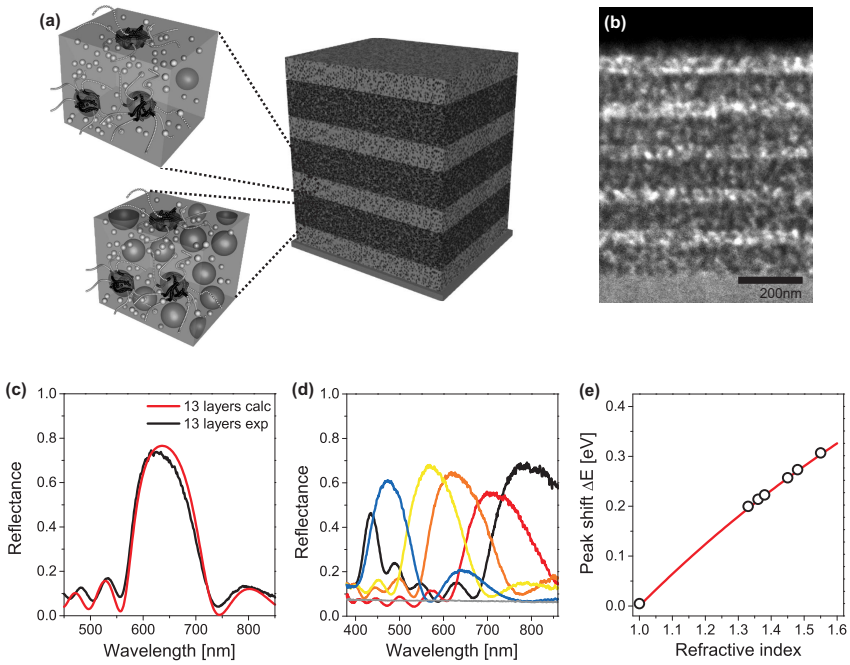

Figure 2. **Mesoporous Bragg reflectors based on BCP co-assembly. (a)** Two stock solutions with a different TiO_2 to polymer weight ratio serve for the fabrication of high and low porosity layers in a multilayer architecture. Stacks are built-up by the alternating deposition and annealing of layers, followed by a final calcination step to reveal the mesopores. **(b)** Cross-sectional view of a 11-layer TiO_2 stack by transmission electron microscopy (TEM). **(c)** Comparison of experimental reflectance (black) with calculations of an ideally regular stack for 13 layers (red). **(d)** Reflectance of 9-layer MDBRs, where the thickness of the five high refractive layers was kept constant while the thickness of the low refractive layers was varied between 78 nm and 292 nm to manipulate the optical response throughout the visible spectrum. **(e)** Corresponding shift of the Bragg peak position after pore infiltration with a variety of different liquids, illustrating full accessibility of the pores through the stack. The grey line corresponds to the theoretical shift of the Bragg peak calculated by a Bruggeman effective medium approximation. *a) Reproduced with permission from reference.[21] Copyright 2011 International Society for Optics and Photonics SPIE. b), d), e) Adapted with permission from reference.[22] Copyright 2011 Wiley. c) Adapted with permission from reference.[23] Copyright 2011 International Society for Optics and Photonics SPIE.*

MDBRs with various functionalizations enables the detection and discrimination of different vapor species such as small molecules and bacteria volatiles.[13] It is important to note that despite limitations in the specificity of the response, a combinatorial approach may allow very accurate sensing by 2D principal component analysis.[14] The coupling of MDBRs to surface layers[15] and resonance cavities[16] facilitates sensing with even greater accuracy.

Material routes towards MDBRs are numerous. Initial attempts were based on porous silicon where the etching conditions were periodically changed to realize a dielectric 1D lattice based on alternating porosities. Solution-processed MDBRs were subsequently introduced by spin coating of BCP co-assembled porous TiO_2 and SiO_2 layers.[5] This approach allowed for better structure control of the porous networks but processing was extremely time consuming with fabrication times up to several days for each individual layer of the stack.[6] A less complex route to form inorganic porous networks in thin films is by the random packing of nanoparticles (NPs).[17,18] While the optical properties of the stack can be tuned by film thickness and choice of the materials based of the constituting layers (e.g. TiO_2 and SiO_2), control over other key parameters as discussed in Figure 1a remains difficult. The random-close packing of somewhat polydisperse NPs results in a rather random pore size distribution and allows only limited control over the porosity by changing the NP size and adding sacrificial filler.[19,20] While many promising proof-of-concepts have been demonstrated by porous silicon and NP-based MDBRs, greater control over pore size and pore accessibility would enable improved functioning and versatility.

We have recently presented a new fast forward route for the fabrication of MDBRs which relies on the co-assembly of TiO_2 (or other inorganic material) by the BCP PI-*b*-PEO. The interplay between the structure-

directing organic host and the co-assembled inorganic guest allows fine tuning of porosity and thus refractive index in the outcome material, simply by changing the ratio between organics and inorganics in the initial solution. As shown in Figure 2a, sequential film deposition and annealing enables multilayer stacking and the build-up of a MDBR. A cross-section of the multilayer stack after removal of the organic material by high temperature calcination is imaged by TEM in Figure 2b. Note that the contrast in electron density within the TiO_2 stack is solely due to the alternating porosity.

We have evaluated the quality of the multilayer stack by comparing experimental results to the expected behavior for an ideal dielectric lattice. Herefore, the optical properties of a single high and low porosity layer were determined by ellipsometry. The multilayer response of a perfect lattice was then modeled with a home-built Matlab algorithm that is based on Rouard's technique.[24] The resemblance between theory and experiments, exemplarily shown in Figure 2c for a 13-layer stack, illustrates the high quality of the outcome MDBRs, which we associate to the well defined optical interfaces, as well as the highly reproducible thickness and refractive index of the layers. In Figure 2d, the reflectance of a variety of 9-layer MDBRs is shown. In order to tune the characteristic reflectance peak from $\approx 475\,\text{nm}$ to $\approx 800\,\text{nm}$, i.e. throughout the visible spectrum, the thickness of the high porosity layers was varied between 78 nm and 292 nm, while the five low porosity layers were kept constant at $\approx 75\,\text{nm}$. The accessibility of the pores throughout the network is crucial for precise functioning in (bio-)chemical sensing. To this end, we have infiltrated the network with solvents of various refractive indices and compared the optical shift to an expected behavior based on effective medium approximation.[25] As shown in Figure 2e, the peak shift follows closely the expected behavior, revealing an accessible relative layer volume of 0.265 and 0.540 for the low and high porosity layer, respectively.

A BCP co-assembly route as presented here offers several advantages over the state-of-the-art. It decouples important parameters in MDBR stack design, porosity and pore size, and allows both properties to be tuned in a wide parameters space. Further is the pore size distribution in comparison to random networks of NPs narrow and controllable by the molecular weight of the pore forming polymer block.[8]

3. SOFT MATTER DESIGN PRINCIPLES FOR PHOTOVOLTAICS

A common component of high performance photovoltaic devices with moderate extinction coefficient in the light absorbing layer is the integration of optical elements that increase the photon path length. In excitonic solar cells (ESCs), such as dye-sensitized solar cells or hybrid solar cells, this is commonly realized by the addition of scattering objects of several hundred nanometers in size.[26,27] A variety of concepts exist, where the scattering particles are positioned either within or on top of the working electrode.[28,29] An optimal scattering design will depend, among others, on the electrode thickness and electron diffusion length.[30] Generally the inclusion of scattering particles proves beneficial for enhanced light absorption, yet, diffuse scattering occurs over a broad spectral range and has the detrimental effect of turning the cells opaque. This deprives ESCs from having a characteristic color, which is a unique selling point and of high potential for integrated architecture.[31]

In contrast, device architectures that incorporate structural order in form of 3D or 1D PCs can lead to the localization of light in specific parts of the spectrum, while retaining the cell's transparency in others.[32,33] In a double layer configuration, where the photoactive layer is sandwiched between the transparent conductive electrode and the PC, an increase in absorbance throughout the region of the photonic band gap of the PC has been proposed. This is associated to light reflection at the PC as well as the formation of resonant modes that lead to a retardation of the photon group velocity.[32] In Figure 3a we compare a classic device architecture of a dye-sensitized solar cell to device configurations where a 3D or 1D PC are integrated. The experimental realization of a double layer structure is, however, difficult. Challenges include the fabrication of a PC on top of a mesoporous photoactive layer as well as the provision of a smooth interface between the layers.[34,35]

We have recently introduced two routes that allow the integration of a PC into an ESC. In the previous section we have shown a BCP co-assembly route to a MDBR, i.e. a 1D PC.[22,23] NP-based MDBRs have been successfully integrated to ESCs, with significant effect on light absorption and overall device efficiency.[10,36,37] As previously discussed, the refractive index lattice in the NP-based MDBRs is realized by the sequential deposition of TiO_2 and SiO_2 NP layers.[18] The use of SiO_2 as the low refractive building block makes the stack non-conducting and thus prevents contribution to light absorption and conversion in the overall device. While certain NP-based routes

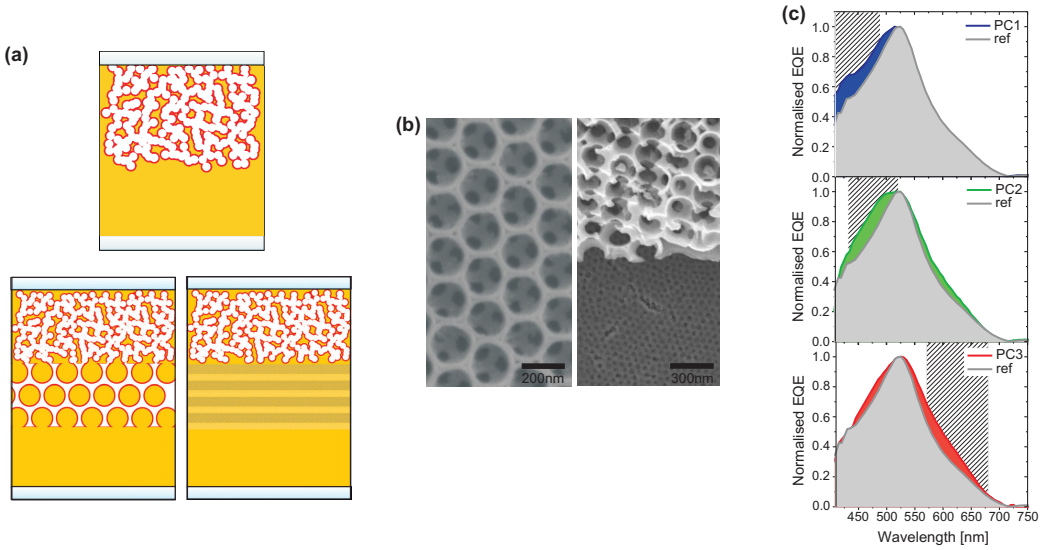

Figure 3. **Photonic crystal-enhanced light absorption in dye-sensitized solar cells. (a)** Conventional device architecture, consisting of a mesoporous electron conducting network of high surface area that is coated with a monolayer of light-absorbing dye molecules and surrounded by a regenerating medium (top). Coupling of the high surface area layer to a 3D or 1D PC in a double layer configuration allows enhanced light harvesting throughout the photonic band gap due to the creation of resonance modes and as well as back reflection. **(b)** SEM images of an inverse opal TiO_2 3D PC(left), which is coupled to a high surface area underlayer (right). **(c)** EQE of double layer arrays compared to reference devices without PC but a similar surface area (PC1 and PC3). The patterned area illustrates the photonic band gap of the 3D in the assembled device. *a) Adapted with permission from reference.*[23] *Copyright 2011 International Society for Optics and Photonics SPIE. b), c) Adapted with permission from reference.*[7]

allow the fabrication of conducing MDBRs,[19,38] the lack of control over pore size and pore accessibility limits mass transport through the porous network and infiltration for solid state devices.[39]

Another approach that we recently presented is the coupling of a 3D PC to a porous underlayer, which is based on a combination of colloidal self-assembly and BCP co-assembly.[7] In our route, the mesoporous underlayer is fabricated by the co-assembly of BCPs and TiO_2 sol. Before calcination, the hybrid layer is nonporous and thus unaffected by the fabrication of a PC top layer, which is typically carried out by evaporation-induced self-assembly of colloids and subsequent infiltration by chemical vapor deposition of TiO_2 . The morphology of the double layer structure as revealed by scanning electron microscopy (SEM) is shown in Figure 3b. Several important aspects for reliable functioning are discernible: the deposition and filing of the colloidal template has been successful, the interface between the two layers is smooth and the layers are well interconnected with fully accessible pores. The effect of the PC top layer on the device functioning of fully assembled dye-sensitized solar cells is shown in Figure 3c. The normalized photon-to-electron conversion efficiency (EQE) of double layer devices incorporating 3D PCs with different photonic band gaps (indicated by the patterned areas) are compared to the absorption of reference cells without a PC but a thicker mesoporous layer to ensure similar overall surface area. The normalized EQE moves closely along the action spectrum of the PC top layer, demonstrating that the absorption spectrum of the device is strongly influenced by the functioning of the PC. From scaling laws, we anticipate scattering at PC defects to play only a minor role in the observed behavior and thus relate the effect largely to back reflection and the build-up of resonance modes. Please see references[7,21] for a full discussion.

Besides enhancing light harvesting by 1D and 3D PCs, BCP co-assembly also enabled us to create novel electrode architectures in photovoltaic devices.[40–43] Morphological control on the 10 nm length scale allowed us to probe the structure-function relationship in dye-sensitized solar cells and improve charge carrier transport properties through crystal growth under confinement.[44–47]

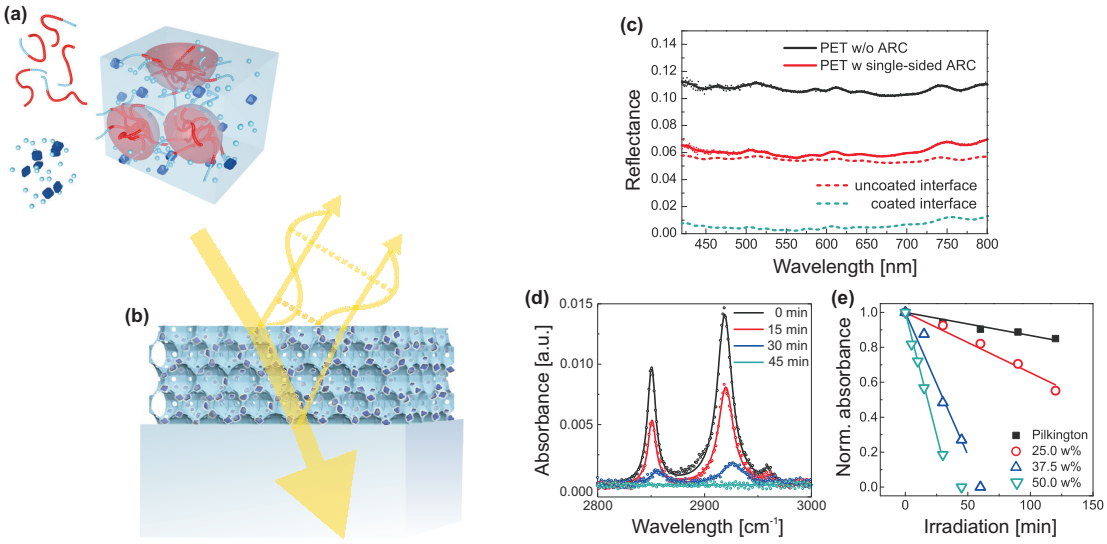

Figure 4. **Self-cleaning antireflective optical coatings. (a)** Compatibilized photocatalytic TiO_2 nanocrystals are co-assembled with PI-*b*-PEO BCP and silica-based sol. **(b)** Thin film processing, low-temperature annealing and subsequent oxygen plasma leads to an inorganic inverse opal-type structure in which the TiO_2 nanocrystals are dispersed. Phase and amplitude matching of the optical coating results destructive interference of reflected light, i.e. enhanced transmission, while the embedded photocatalytic hot spots prevent contamination of the ARC. **(c)** The low temperature fabrication route ($< 130\,^{\circ}C$) allows film processing onto flexible and low-cost PET substrates with near optimum optical properties. **(d)** FTIR spectra, illustrating the decomposition of stearic acid as a function of irradiation time under simulated sunlight (AM1.5). **(e)** Decay of the integrated peak area with time for different TiO_2 loadings. The decay of the commercially available self-cleaning Pilkington Active glass (not antireflective) is shown for comparison. *a) - e) Adapted with permission from reference.*[8]

4. SOFT MATTER DESIGN PRINCIPLES FOR SELF-CLEANING ANTIREFLECTIVE COATINGS

Antireflective coatings (ARCs) to reduce light reflection at interfaces are important for a number of applications in optoelectronics and architecture. ARCs are typically interference-based and rely on amplitude and phase matching of light reflected at its interfaces. This requires the optical thickness to be $\lambda/4$ for a given wavelength and angle of incidence and the effective refractive index of the ARC (n_{AR}) to be the square root of the underlying substrate.[48] Common substrates such glass or polyethylene terephthalate (PET) with a refractive index of around 1.5 therefore require unrealistically low values of $n_{ARC} \approx 1.22$. This is typically solved by introducing porosity on the sub-wavelength scale. The effective refractive index of the material-air composite can then be derived from effective medium approximations, such as the Bruggeman model.[49] Material approaches to porous ARCs are numerous and include polymer phase separation on the sub-100 nm scale with subsequent removal of one of the phases,[50,51] random dense packing of NPs,[52] as well as colloidal approaches.[53–56] While these routes lead to high performance optical coatings, commercial implementation is held up by their susceptibility to contamination and thus decay in functioning. This could be prevented by photocatalytic self-cleaning, i.e. the decomposition of organic contaminants by light-induced redox-reactions.[57] The inclusion of photocatalytic hot spots is challenged by their high refractive index ($n_{TiO_2} > 2.5$[58]), which limits the amount of photocatalytic material that can be included in a self-cleaning ARC while still meeting the requirements in n_{ARC}. Previous approaches included the surface coating of a colloidal-based ARC with TiO_2,[59] the co-deposition of TiO_2 and SiO_2 NPs to form a porous ARC,[60] the synthesis of SiO_2 / TiO_2 core-shell particles,[61] as well as a double layer structure of low refractive index SiO_2 and TiO_2.[62–64] Yet, all of these approaches only achieved optimum optical performance for a very low TiO_2 loading and were incompatible with transparent plastics due to processing temperatures of above $400\,^{\circ}C$.

We have recently established a simple method for the manufacture of robust ARCs with greatly improved

self-cleaning capabilities.[8] As shown in Figure 4a, our strategy relies on BCP co-assembly of a combination of silica-based sol and preformed TiO_2 nanocrystals. The spontaneous dense packing of copolymer micelles during the film formation process, followed by condensation of the silica-based matrix during film annealing and subsequent removal of the organic host, results in an inverse opal-type silica morphology that is loaded with TiO_2 photocatalytic hot-spots. The micellar arrangement effectively represents the densest packing of sacrificial material. The resulting ultra low volume fraction of the inorganic material enables a high loading of the network with TiO_2 nanocrystals and thus a simultaneous matching of the requirements for self-cleaning (high relative content of photocatalytic material, here up to 50 %) and antireflection ($n_{ARC} \approx 1.22$). Our method requires only moderate annealing temperatures ($< 150°C$) and can therefore be processed onto plastic substrates. The resulting optical properties are shown in Figure 4c, where the reflectance of an uncoated PET foil (PET-0s) is compared to a sample that was coated on one side with a self-cleaning ARC (PET-1s). By simple interfacial analysis with $R_{PET-0s} = A + ((1 - A) \times A)$ and $R_{PET-1s} = B + ((1 - B) \times A)$, one can derived the reflectance R of an uncoated (A) and a coated PET interface (B). The spectral traces suggest a near ideal broad-band antireflective response with up to ≈ 5.2 % reduction in reflectance for each coated interface. The photocatalytic efficiency of our coatings can be studied by the decomposition of stearic acid as a function of irradiation time under simulated sunlight (AM1.5). Stearic acid is a widely used model molecule which assembles as a monolayer onto the coating and can be traced by Fourier transform infrared spectroscopy (FTIR), shown in Figure 4d for an ARC with 50 w% TiO_2. The role of the TiO_2 loading is further evidenced in Figure 4e, where the decay in normalized absorbance is compared for ARCs containing 25-50 w% TiO_2. Interestingly, our coatings clearly outperform commercially available self-cleaning glass that is not antireflective and thus less constrained in its composition.

5. CONCLUSIONS

This perspective was written to illustrate the rich tool box that soft matter and in particular BCP co-assembly offers for the design of inorganic nanoarchitectures with tunable photonic response. Detailed control over pore accessibility, pore architecture, refractive index tuning, film thickness and multilayer stacking in thin films allowed to create highly ordered multilayer stacks with a near optimum regularity and pore accessibility. These MDBRs are highly promising for (bio-)chemical sensing, enhanced light harvesting in photovoltaics and other optoelectronic applications, such as hybrid lasers.[65] The combination of evaporation-induced self-assembly of colloids and BCP co-assembly enabled a double layer architecture for use in dye-sensitized solar cells where the 3D PC top layer has a significant impact on the overall photon-to-electron conversion of the device. The material arrangement in the presented BCP co-assembly is based on the formation of micelles in solution and subsequent micellar packing upon solvent evaporation during thin film development. This allows to create inverse-opal type architectures with ultrahigh porosities, opening up a route antireflective coatings with outstanding photocatalytic self-cleaning due to the doping with high refractive index hot spots. Beyond BCP co-assembly we have recently also developed alternative routes to porous thin film architectures with interesting photonic properties. This includes BCP self-assembly near thermodynamic equilibrium and subsequent infiltration with inorganic material, resulting in ZnO gyroid networks[66] and chiral metamaterials made of gold,[67] as well as a synthetic analogue to abalone nacre with similar photonic response and mechanic toughness.[68]

ACKNOWLEDGMENTS

S.G. is grateful for support by the German National Academy of Sciences Leopoldina, Fellowship LPDS2012-13.

REFERENCES

[1] Hamley, I., "Nanotechnology with soft materials," *Angewandte Chemie - Int. Ed.* **42**(15), 1692–1712 (2003).
[2] Templin, M., Franck, A., DuChesne, A., Leist, H., Zhang, Y., Ulrich, R., Schädler, V., and Wiesner, U., "Organically modified aluminosilicate mesostructures from block copolymer phases," *Science* **278**(5344), 1795–1798 (1997).
[3] Zhao, D., Feng, J., Huo, Q., Melosh, N., Fredrickson, G., Chmelka, B., and Stucky, G., "Triblock copolymer syntheses of mesoporous silica with periodic 50 to 300 angstrom pores," *Science* **279**(5350), 548–552 (1998).
[4] Guldin, S., Docampo, P., Stefik, M., Kamita, G., Wiesner, U., Snaith, H., and Steiner, U., "Layer-by-layer formation of block copolymer derived TiO_2 for solid state dye-sensitized solar cells," *Small* **8**(3), 432–440 (2012).

[5] Choi, S., Mamak, M., von Freymann, G., Chopra, N., and Ozin, G., "Mesoporous Bragg stack color tunable sensors," *Nano Letters* **6**(11), 2456–2461 (2006).
[6] Fuertes, M. C., Lopez-Alcaraz, F. J., Marchi, M. C., Troiani, H. E., Luca, V., Míguez, H., and Arturo Soler-Illia, G. J. d. A., "Photonic crystals from ordered mesoporous thin-film functional building blocks," *Advanced Functional Materials* **17**(8), 1247–1254 (2007).
[7] Guldin, S., Hüttner, S., Kolle, M., Welland, M., Müller-Buschbaum, P., Friend, R., Steiner, U., and Tetreault, N., "Dye-sensitized solar cell based on a three-dimensional photonic crystal," *Nano Letters* **10**(7), 2303–2309 (2010).
[8] Guldin, S., Kohn, P., Stefik, M., Song, J., Divitini, G., Ecarla, F., Ducati, C., Wiesner, U., and Steiner, U., "Self-Cleaning Antireflective Optical Coatings," *Nano Letters* **13**(11), 5329–5335 (2013).
[9] Bonifacio, L., Lotsch, B., Puzzo, D., Scotognella, F., and Ozin, G., "Stacking the nanochemistry deck: structural and compositional diversity in one-dimensional photonic crystals," *Advanced Materials* **21**(16), 1641–1646 (2009).
[10] Calvo, M., Colodrero, S., Hidalgo, N., Lozano, G., Lopez-Lopez, C., Sanchez-Sobrado, O., and Míguez, H., "Porous one dimensional photonic crystals: novel multifunctional materials for environmental and energy applications," *Energy & Environmental Science* **4**, 4800–4812 (2011).
[11] Fuertes, C., Colodrero, S., Lozano, G., González-Elipe, A., Grosso, D., Boissière, C., Sánchez, C., Soler-Illia, G. J. d. A., and Míguez, H., "Sorption properties of mesoporous multilayer thin films," *Journal of Physical Chemistry C* **106**, 3157–3163 (2008).
[12] Lin, V., Motesharei, K., Dancil, K., Sailor, M., and Ghadiri, M., "A porous silicon-based optical interferometric biosensor," *Science* **278**(5339), 840–843 (1997).
[13] Bonifacio, L. D., Puzzo, D. P., Breslav, S., Willey, B. M., McGeer, A., and Ozin, G. A., "Towards the photonic nose: a novel platform for molecule and bacteria identification," *Advanced Materials* **22**(12), 1351–4 (2010).
[14] Jolliffe, I., [*Principal Component Analysis*], Springer, 2nd ed. (2002).
[15] Hidalgo, N., Calvo, M. E., and Míguez, H., "Mesostructured thin films as responsive optical coatings of photonic crystals.," *Small* **5**(20), 2309–15 (2009).
[16] Sánchez-Sobrado, O., Calvo, M. E., Núñez, N., Ocaña, M., Lozano, G., and Míguez, H., "Environmentally responsive nanoparticle-based luminescent optical resonators," *Nanoscale* **2**(6), 936 (2010).
[17] Wu, Z., Lee, D., Rubner, M. F., and Cohen, R. E., "Structural color in porous, superhydrophilic, and self-cleaning SiO_2 /TiO_2 Bragg stacks.," *Small* **3**(8), 1445–51 (2007).
[18] Colodrero, S., Ocana, M., and Míguez, H., "Nanoparticle-based one-dimensional photonic crystals," *Langmuir* **24**(9), 4430–4434 (2008).
[19] Calvo, M. E., Colodrero, S., Rojas, T. C., Anta, J. A., Ocana, M., and Míguez, H., "Photoconducting Bragg mirrors based on TiO_2 nanoparticle multilayers," *Advanced Functional Materials* **18**, 2708–2715 (2008).
[20] Lopez-Lopez, C., Colodrero, S., Raga, S. R., Lindstrom, H., Fabregat-Santiago, F., Bisquert, J., and Miguez, H., "Enhanced diffusion through porous nanoparticle optical multilayers," *Journal Of Materials Chemistry* **22**(5), 1751–1757 (2012).
[21] Guldin, S., Docampo, P., Hüttner, S., Kohn, P., Stefik, M., H.J., S., Wiesner, U., and Steiner, U., "Self-assembly as a design tool for the integration of photonic structures into excitonic solar cells," *Proceedings of the SPIE* **8111, DOI: 10.1117/12.893798** (2011).
[22] Guldin, S., Kolle, M., Stefik, M., Langford, R., Eder, D., Wiesner, U., and Steiner, U., "Tunable mesoporous bragg reflectors based on block-copolymer self-assembly," *Advanced Materials* **23**(32), 3664–3668 (2011).
[23] Guldin, S., Kolle, M., Stefik, M., Wiesner, U., and Steiner, U., "Mesoporous Bragg reflectors - block-copolymer self-assembly leads to building blocks with well defined continuous pores and high control over optical properties," *Proceedings of the SPIE* **8095, DOI: 10.1117/12.893818** (2011).
[24] Heavens, O., [*The optical properties of thin solid films*], Dover (1992).
[25] Hutchinson, N. J., Coquil, T., Navid, A., and Pilon, L., "Effective optical properties of highly ordered mesoporous thin films," *Thin Solid Films* **518**(8), 2141–2146 (2010).
[26] Chiba, Y., Islam, A., Watanabe, Y., Komiya, R., Koide, N., and Han, L., "Dye-sensitized solar cells with conversion efficiency of 11.1%," *Japanese Journal Of Applied Physics Part 2-Letters & Express Letters* **45**(24-28), L638–L640 (2006).
[27] Yella, A., Lee, H.-W., Tsao, H., Yi, C., Chandiran, A., Nazeeruddin, M., Diau, E.-G., Yeh, C.-Y., Zakeeruddin, S., and Grätzel, M., "Porphyrin-sensitized solar cells with cobalt (II/III)-based redox electrolyte exceed 12 percent efficiency," *Science* **334**(6056), 629–634 (2011).
[28] Wang, Z., Kawauchi, H., Kashima, T., and Arakawa, H., "Significant influence of TiO_2 photoelectrode morphology on the energy conversion efficiency of N719 dye-sensitized solar cell," *Coordination Chemistry Reviews* **248**(13-14), 1381–1389 (2004).
[29] Hore, S., Vetter, C., Kern, R., Smit, H., and Hinsch, A., "Influence of scattering layers on efficiency of dye-sensitized solar cells," *Solar Energy Materials and Solar Cells* **90**(9), 1176–1188 (2006).

[30] Enrique Galvez, F., Kemppainen, E., Miguez, H., and Halme, J., "Effect of diffuse light scattering designs on the efficiency of dye solar cells: an integral optical and electrical description," *Journal Of Physical Chemistry C* **116**(21), 11426–11433 (2012).
[31] Yoon, S., Tak, S., Kim, J., Jun, Y., Kang, K., and Park, J., "Application of transparent dye-sensitized solar cells to building integrated photovoltaic systems," *Building And Environment* **46**(10), 1899–1904 (2011).
[32] Mihi, A. and Míguez, H., "Origin of light-harvesting enhancement in colloidal-photonic-crystal-based dye-sensitized solar cells," *Journal Of Physical Chemistry B* **109**(33), 15968–15976 (2005).
[33] Colodrero, S., Mihi, A., Anta, J. A., Ocaña, M., and Míguez, H., "Experimental demonstration of the mechanism of light harvesting enhancement in photonic-crystal-based dye-sensitized solar cells," *Journal Of Physical Chemistry C* **113**, 1150–1154 (2009).
[34] Nishimura, S., Abrams, N., Lewis, B., Halaoui, L., Mallouk, T., Benkstein, K., van de Lagemaat, J., and Frank, A., "Standing wave enhancement of red absorbance and photocurrent in dye-sensitized titanium dioxide photoelectrodes coupled to photonic crystals," *Journal Of The American Chemical Society* **125**(20), 6306–6310 (2003).
[35] Lee, S.-H. A., Abrams, N. M., Hoertz, P. G., Barber, G. D., Halaoui, L. I., and Mallouk, T. E., "Coupling of titania inverse opals to nanocrystalline titania layers in dye-sensitized solar cells," *Journal Of Physical Chemistry B* **112**(46), 14415–14421 (2008).
[36] Colodrero, S., Mihi, A., Haggman, L., Ocaña, M., Boschloo, G., Hagfeldt, A., and Míguez, H., "Porous one-dimensional photonic crystals improve the power-conversion efficiency of dye-sensitized solar cells," *Advanced Materials* **21**(7), 764770 (2009).
[37] Colonna, D., Colodrero, S., Lindstrom, H., Di Carlo, A., and Miguez, H., "Introducing structural colour in DSCs by using photonic crystals: interplay between conversion efficiency and optical properties," *Energy & Environmental Science* **5**(8), 8238–8243 (2012).
[38] Anaya, M., Calvo, M. E., Luque-Raigon, J. M., and Miguez, H., "Resonant photocurrent generation in dye-sensitized periodically nanostructured photoconductors by optical field confinement effects," *Journal Of The American Chemical Society* **135**(21), 7803–7806 (2013).
[39] Docampo, P., Guldin, S., Leijtens, T., Noel, N., Steiner, U., and Snaith, H., "Lessons learned: from dye-sensitised solar cells to all-solid-state hybrid devices," *Advanced Materials* **DOI: 10.1002/adma.201400486**, (2014).
[40] Nedelcu, M., Lee, J., Crossland, E., Warren, S., Orilall, M., Guldin, S., Hüttner, S., Ducati, C., Eder, D., Wiesner, U., Steiner, U., and Snaith, H., "Block copolymer directed synthesis of mesoporous TiO_2 for dye-sensitized solar cells," *Soft Matter* **5**, 134–139 (2009).
[41] Nedelcu, M., Guldin, S., Orilall, M., Lee, J., Hüttner, S., Crossland, E., Warren, S., Ducati, C., Laity, P., Eder, D., Wiesner, U., Steiner, U., and Snaith, H., "Monolithic route to efficient dye-sensitized solar cells employing diblock copolymers for mesoporous tio_2," *Journal Of Materials Chemistry* **20**, 1261–1268 (2010).
[42] Docampo, P., Guldin, S., Stefik, M., Tiwana, P., Orilall, M., Hüttner, S., Sai, H., Wiesner, U., Steiner, U., and Snaith, H., "Control of solid-state dye-sensitized solar cell performance by block-copolymer-directed TiO_2 synthesis," *Advanced Functional Materials* **20**(11), 1787 – 1796 (2010).
[43] Docampo, P., Stefik, M., Guldin, S., Yufa, N., Gunning, R., Wiesner, U., Steiner, U., and Snaith, H., "Triblock terpolymer directed self-assembly of mesoporous TiO_2 - high performance photoanodes for solid state dye-sensitized solar cells," *Advanced Energy Materials* **2**, 676–682 (2012).
[44] Guldin, S., Hüttner, S., Tiwana, P., Orilall, M., Ülgüt, B., Stefik, M., Docampo, P., Kolle, M., Divitini, G., Ducati, C., Redfern, S., Snaith, H., Wiesner, U., Eder, D., and Steiner, U., "Improved conductivity in dye-sensitised solar cells through block-copolymer confined TiO_2 crystallisation," *Energy & Environmental Science* **4**(1), 225–233 (2011).
[45] Docampo, P., Hey, A., Guldin, S., Gunning, R., Steiner, U., and Snaith, H., "Pore filling of spiro-ometad in solid-state dye-sensitized solar cells determined via optical reflectometry," *Advanced Functional Materials* **22**, 5010–5019 (2012).
[46] Kohn, P., Pathak, S., Stefik, M., Ducati, C., Wiesner, U., Steiner, U., and Guldin, S., "Low temperature crystallisation of mesoporous TiO_2 ," *Nanoscale* **5**(21), 10518–10524 (2013).
[47] Docampo, P., Guldin, S., Steiner, U., and Snaith, H., "Charge transport limitations in self-assembled TiO_2 photoanodes for dye-sensitized solar cells," *The Journal of Physical Chemistry Letters* **4**, 698–703 (2013).
[48] Macleod, H., [*Thin film optical filters*], Institute of Physics Publishing, 3rd ed. (2001).
[49] Bruggeman, D., "Berechnung verschiedener physikalischer Konstanten von heterogenen Substanzen. i. Dielektrizitätskonstanten und Leitfähigkeiten der Mischkörper aus isotropen Substanzen," *Ann. d. Physik* **416**(7), 636 (1935).
[50] Walheim, S., Schäffer, E., Mlynek, J., and Steiner, U., "Nanophase-separated polymer films as high-performance antireflection coatings," *Science* **283**(5401), 520–522 (1999).
[51] Kim, S., Cho, J., and Char, K., "Thermally stable antireflective coatings based on nanoporous organosilicate thin films.," *Langmuir* **23**(12), 6737–43 (2007).
[52] Thomas, I. M., "Method for the preparation of porous silica antireflection coatings varying in refractive index from 1.22 to 1.44.," *Applied Optics* **31**(28), 6145–9 (1992).

[53] Hattori, H., "Anti-reflection surface with particle coating deposited by electrostatic attraction," *Advanced Materials* **13**(1), 51–54 (2001).
[54] Guillemot, F., Brunet-Bruneau, A., Bourgeat-Lami, E., Gacoin, T., Barthel, E., and Boilot, J.-P., "Latex-Templated Silica Films: Tailoring Porosity to Get a Stable Low-Refractive Index," *Chemistry Of Materials* **22**(9), 2822–2828 (2010).
[55] Du, Y., Luna, L. E., Tan, W. S., Rubner, M. F., and Cohen, R. E., "Hollow silica nanoparticles in uv-visible antireflection coatings for poly(methyl methacrylate) substrates," *ACS Nano* **4**(7), 4308–4316 (2010).
[56] Moghal, J., Kobler, J., Sauer, J., Best, J., Gardener, M., Watt, A. A. R., and Wakefield, G., "High-performance, single-layer antireflective optical coatings comprising mesoporous silica nanoparticles," *ACS Applied Materials & Interfaces* **4**(2), 854–859 (2012).
[57] Parkin, I. P. and Palgrave, R. G., "Self-cleaning coatings," *J. Mater. Chem.* **15**, 1689–1695 (2005).
[58] Tang, H., Berger, H., Schmid, P., and F., L., "Optical properties of anatase TiO_2," *Solid State Commun.* **92**(3), 267–271 (1994).
[59] Zhang, X.-T., Sato, O., Taguchi, M., Einaga, Y., Murakami, T., and Fujishima, A., "Self-cleaning particle coating with antireflection properties," *Chemistry Materials* **17**(3), 696–700 (2005).
[60] Lee, D., Rubner, M. F., and Cohen, R. E., "All-nanoparticle thin-film coatings.," *Nano Letters* **6**(10), 2305–12 (2006).
[61] Li, X. and He, J., "Synthesis of raspberry-like SiO_2 -TiO_2 nanoparticles toward antireflective and self-cleaning coatings," *ACS Applied Materials & Interfaces* **5**(11), 5282–5290 (2013).
[62] Zhang, X., Fujishima, A., Jin, M., Emeline, A. V., and Murakami, T., "Double-layered TiO_2-SiO_2 nanostructured films with self-cleaning and antireflective properties.," *Journal of Physical Chemistry B* **110**(50), 25142–25148 (2006).
[63] Liu, Z., Zhang, X., Murakami, T., and Fujishima, A., "Sol-gel SiO_2/TiO_2 bilayer films with self-cleaning and antireflection properties," *Solar Energy Materials And Solar Cells* **92**(11), 1434–1438 (2008).
[64] Faustini, M., Nicole, L., Boissiere, C., Innocenzi, P., Sanchez, C., and Grosso, D., "Hydrophobic, antireflective, self-cleaning, and antifogging sol-gel coatings: an example of multifunctional nanostructured materials for photovoltaic cells," *Chemistry of Materials* **22**(15), 4406–4413 (2010).
[65] Puzzo, D. P., Scotognella, F., Zavelani-Rossi, M., Sebastian, M., Lough, A. J., Manners, I., Lanzani, G., Tubino, R., and Ozin, G. A., "Distributed feedback lasing from a composite poly(phenylene vinylene)-nanoparticle one-dimensional photonic crystal.," *Nano Letters* **9**(12), 4273–8 (2009).
[66] Kim, E., Vaynzof, Y., Sepe, A., Guldin, S., Scherer, M., Cunha, P., Roth, S. V., and Steiner, U., "Gyroid-structured 3d ZnO networks made by atomic layer deposition," *Advanced Functional Materials* **24**(6), 863–872 (2014).
[67] Vignolini, S., Yufa, N. A., Cunha, P. S., Guldin, S., Rushkin, I., Stefik, M., Hur, K., Wiesner, U., Baumberg, J. J., and Steiner, U., "A 3D optical metamaterial made by self-assembly," *Advanced Materials* **24**, OP23–OP27 (2012).
[68] Finnemore, A., Cunha, P., Shean, T., Vignolini, S., Guldin, S., Oyen, M., and Steiner, U., "Biomimetic layer-by-layer assembly of artificial nacre," *Nature Communications* **3**, 966 (2012).